



Satellite-based measurements of gravity wave-induced midlatitude plasma density perturbations

G. D. Earle,¹ A. M. Musumba,¹ and Sharon L. Vadas²

Received 27 August 2007; revised 15 October 2007; accepted 19 November 2007; published 12 March 2008.

[1] Large amplitude anticorrelated wave structures appear at midlatitudes in the nighttime ionospheric plasma and neutral density measurements made at altitudes between 250 and 300 km by the Dynamics Explorer-2 satellite. The wavelengths along the satellite orbit track are generally longer than a hundred kilometers, and the vertical perturbation velocities are about 20 m/s. These characteristics are consistent with plasma motions driven by gravity waves in the neutral atmosphere as they propagate upward from lower atmospheric source regions. The altitude and the horizontal wavelengths observed provide in situ empirical validation of a recently developed gravity wave propagation model that includes the effects of both kinematic viscosity and thermal diffusivity at high altitudes.

Citation: Earle, G. D., A. M. Musumba, and S. L. Vadas (2008), Satellite-based measurements of gravity wave-induced midlatitude plasma density perturbations, *J. Geophys. Res.*, 113, A03303, doi:10.1029/2007JA012766.

1. Introduction

[2] Radar and airglow measurements in the thermosphere routinely show signatures consistent with gravity wave-induced perturbations of the ionospheric plasma density [Fukao *et al.*, 1991; Oliver *et al.*, 1997; Kelley *et al.*, 2000]. The horizontal wavelengths, propagation directions, and periodic nature of these waves are well resolved by such techniques. However, these radio and optical observations involve line-of-sight integrated signatures, which complicate determination of specific altitude ranges for the waves as well as estimation of their amplitudes. To garner this information it is necessary to augment the radio and optical measurements using in situ satellites. A few such observations of meso- and large-scale wave structures have previously been made by the Atmospheric Explorer-C (AE-C) and Dynamics Explorer-2 (DE-2) satellites, but these do not focus on mesoscale wave structures in the midlatitude region, and do not include the densities and velocities of both ions and neutral particles [Gross *et al.*, 1984; Hedin and Mayr, 1987; Johnson *et al.*, 1995]. The dearth of such satellite-based observations suggests that the waves do not propagate routinely at satellite altitudes.

[3] Late in the lifetime of the DE-2 satellite its initially elliptical orbit had decayed to a point where it spent significant time at altitudes below 300 km, the nominal height of the peak ionospheric plasma density. During these orbits there are a number of examples of large amplitude

wave structures at nighttime middle magnetic latitudes. Because of the slowly precessing polar orbit all of these observations are at nearly the same local time, but they occur at widespread longitudes, implying that the phenomenon is global in nature.

[4] Large waves on the bottomside of the nighttime ionospheric density profile may be one of the critical precursors that initiate the development of so-called spread-F instabilities at equatorial [Hysell, 2000] and midlatitudes [Earle *et al.*, 2006]. These phenomena are known to cause scintillation across wide radio frequency bands, and can completely disrupt radio frequency communication in the HF and MF bands. At higher frequencies these ionospheric irregularities produce positioning errors on the order of 50 m in GPS-based navigation systems [Yunck, 1993; Dubey *et al.*, 2006]. The source of the gravity waves that are widely held to be responsible for initiating these instabilities may be auroral zone heating, or convective upwelling associated with terrestrial weather systems. The latter mechanism has recently been shown to strongly affect the *F* region ionosphere within the magnetic midlatitude zone [Bishop *et al.*, 2006].

[5] The focus of the present work is to present the DE-2 data and compare the characteristics of the observations with the predictions of a state-of-the-art gravity wave propagation model. These comparisons will illuminate several interesting features of the thermospheric gravity wave environment, while serving as an empirical validation of the theoretical model.

2. Experiment Description

[6] The DE-2 satellite launched on 3 August 1981 into an elliptical orbit with initial apogee and perigee of 1012 and 309 km, respectively. The orbital period of 98 min coupled

¹William B. Hanson Center for Space Sciences, The University of Texas at Dallas, Richardson, Texas, USA.

²NorthWest Research Associates, CoRA Division, Boulder, Colorado, USA.

with the high inclination orbit to provide a relatively slow precession in local time. DE-2 reentered the atmosphere in mid-February 1983, after a useful lifetime of approximately 18 months. All of the measurements shown here are from January 1983, at which time the perigee of the orbit was near 245 km. The DE-2 satellite carried a variety of instruments, but the ones of interest to this study are the duct sensor, wind and temperature spectrometer (WATS), and the ion drift meter (IDM). These measure the relative ion density, neutral wind and temperature, and bulk ion motion, respectively.

[7] The duct sensor instrument measures the ion current to a negatively biased flat collector plate oriented with its normal along the satellite velocity vector. The sampling frequency for the ion current measurement is 64 Hz [Hanson *et al.*, 1981]. Because of its ram-facing orientation on the spacecraft, the ion current to the instrument provides a measure of the relative plasma density along the orbit track. The explicit relationship is

$$I = NevA \quad (1)$$

where I is the current to the sensor in amps, N is the ion density in particles per cubic meter, e is the ion charge in Coulombs, v is the relative velocity between the satellite and the ion population in meters per second, and A is the effective collecting area of the instrument in square meters. The noise level of the instrument is in the nanoamp range, and at typical bottomside ionospheric densities the signal to noise level exceeds one hundred. At the indicated sample rate the spatial separation between consecutive density measurements is approximately 120 meters, which is much smaller than the horizontal wavelengths of the waves under consideration.

3. Data Presentation

[8] The nighttime duct meter data set from the entire 18 month lifetime of DE-2 has been examined for evidence of meso-scale waves at midlatitudes. For purposes of this paper midlatitudes are defined as lying between 20 and 50 degrees magnetic latitude in both hemispheres. This range is sufficient to effectively exclude most of the particle precipitation associated with the auroral zones, while also avoiding influences of low latitude phenomena like equatorial spread F . The middle latitude range is often overlooked in the DE-2 data set, because in examining orbit plots the eye is naturally drawn to the high latitude and equatorial regions, where the highly disturbed structures associated with auroral particle precipitation and equatorial spread F are encountered, respectively.

[9] Figure 1 shows four panels in which are plotted linearly detrended ion density data from the duct meter. All panels share a common time axis that shows satellite time in seconds. The orbit numbers, satellite locations, and universal times corresponding to the beginning of each observation are also shown. The plots show the best four cases of wave events at midlatitudes for which long, continuous data sets are available. All four cases are from the southern hemisphere at altitudes below 300 km, and in all cases the satellite is traveling equatorward during the measurement interval. The fact that all four measurements

are from roughly the same local time in the same hemisphere is a consequence of the slowly precessing, slightly elliptical orbit. In other words, the orbital characteristics are such that the satellite consistently passes below the F peak in the southern hemisphere at this late stage in its life, and its polar orbit leads to a slow precession in time, which results in observations clustered near 0230 LT. Despite these limitations, the range of longitudes covered by the observations suggests that the events are global in nature.

[10] Of the four orbits shown in Figure 1, only orbit 8092 shows any evidence of particle precipitation (centered near $t = 100$ s). All four panels show large wave amplitudes at wavelengths longer than 100 km. The average amplitude of the plasma density fluctuations is about 30%, although some perturbations are over three times larger. None of these events occur in association with strong magnetic storms; all four are from quiet or mildly disturbed periods. The sum of the K_p values during the 12 h preceding each event were 13^- , 13^+ , 9 , and 9^+ (in order of orbit number).

[11] Figure 2 shows a more detailed view of orbit 8140. The perturbation of the ion density is replotted in the top panel, while the second panel shows the corresponding neutral density fluctuations. The third and fourth panels show the linearly detrended ion and neutral vertical velocities in units of m/s, respectively. Throughout this paper the term vertical implies toward the zenith, independent of the magnetic field direction. The ion and neutral velocity data are from the Ion Drift Meter (IDM) and the Wind and Temperature Spectrometer (WATS) instruments aboard DE-2, respectively [Heelis *et al.*, 1981; Spencer *et al.*, 1981]. The instruments measure the arrival angle of the ionized and neutral gases relative to the satellite velocity track. All three instruments are electrically independent sensors, so there is little chance that the correlations shown in the figure result from cross-talk between instruments.

[12] The behavior shown in the figure is typical of all four orbits. Comparison of the density data in the top two panels shows that the ion and neutral densities have similar wavelike characteristics, but are anti-correlated and have very different amplitudes. The vertical ion velocity from the IDM is often anti-correlated with the ion density perturbations, but there are periods (e.g., ~ 175 s) in which different phase offsets occur. The neutral vertical velocity data from the WATS instrument have much lower temporal resolution, but generally appear to lead the neutral density fluctuations by ninety degrees.

[13] The spectral characteristics of the detrended density fluctuations are shown in Figure 3. The satellite velocity has been used to determine the wavelength scale on the abscissa. It is noteworthy that the power level in each of the disturbed spectra changes character rather abruptly for wavelengths longer than 100–200 km. To highlight this, each of the plasma fluctuation spectra (left panels) are superimposed with a line representing the best fit over the 1–10 km wavelength range. In all four cases the power level at wavelengths longer than 150 km is well above this line, and for three of the four cases the increase is several orders of magnitude. It is likely that the single case (orbit 8092) in which the power is least enhanced above the power law line is corrupted by the influence of particle precipitation (see Figure 1), which produces small scale density

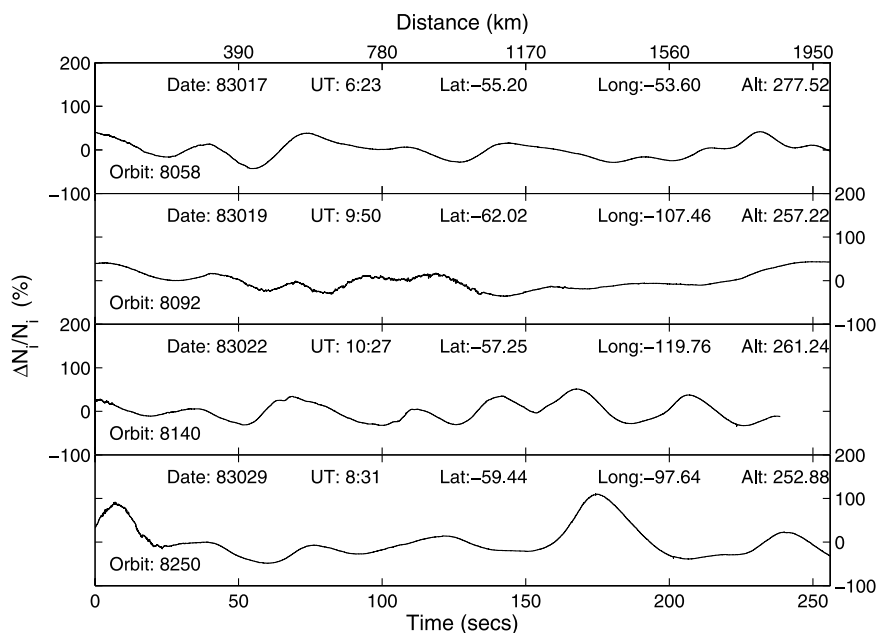


Figure 1. Ion density perturbations in the time domain for four different nighttime midlatitude orbits of the DE-2 satellite. All data have been linearly detrended to highlight the level of the variations. The locations and times shown in each panel correspond to the origin in each graph, with latitude and longitude given in degrees, and altitude in km.

structures that modify the power law. Note that the slope of the power law fit is markedly different in this case, but the other three are very similar.

[14] The neutral density spectra shown in the right panels in Figure 3 are very similar to the plasma density irregularity spectra for the longer wavelengths, but are relatively flat for wavelengths shorter than 100 km. This is probably an artifact of the coarser sampling and higher noise level in the WATS instrument, rather than representative of a geophysical effect. The WATS wind measurements occur at ~ 7 s intervals, and the uncertainty inherent in the absolute wind measurements is ~ 20 m/s. The enhanced power at longer wavelengths is not surprising in the neutral spectra, considering the similarities between plasma and neutral perturbations shown in Figure 2.

[15] The empirical spectra shown in Figure 3 can be directly compared to the predictions of a gravity wave propagation model, shown in Figure 4. *Vadas and Fritts* [2005] derive a complete, anelastic gravity wave dispersion relation that includes kinematic viscosity and thermal conductivity. *Vadas* [2007] applies this dispersion relation and quantifies the dissipative filtering of gravity waves as a function of wavelength and altitude. Figure 4 shows the model thermospheric propagation characteristics for a white noise source of gravity waves with horizontal wavelengths between 10 km and 3000 km. These waves are assumed to result from a source in the lower atmosphere, and to have periods ranging from the buoyancy period (about 5 min) up to six hours. The temperature and density profiles of the neutral atmosphere used in these model runs are taken from the MSISE-90 model [*Hedin*, 1991] for average conditions at the latitudes and local times corresponding to the DE-2 observations. The plots show how the incident white-noise

spectrum of gravity waves are dissipatively filtered as they propagate upward into the lower F region of the ionosphere.

[16] The top two panels in Figure 4 correspond to a case with a stationary background atmosphere, while the bottom two panels correspond to a case where the gravity waves propagate through a thermosphere that has a 150 m/s net horizontal drift. This particular value for the horizontal neutral flow is appropriate for the latitudes and local times of the DE-2 observations, according to the TIME-GCM model (*Han-Li Liu*, personal communication). Panels a and

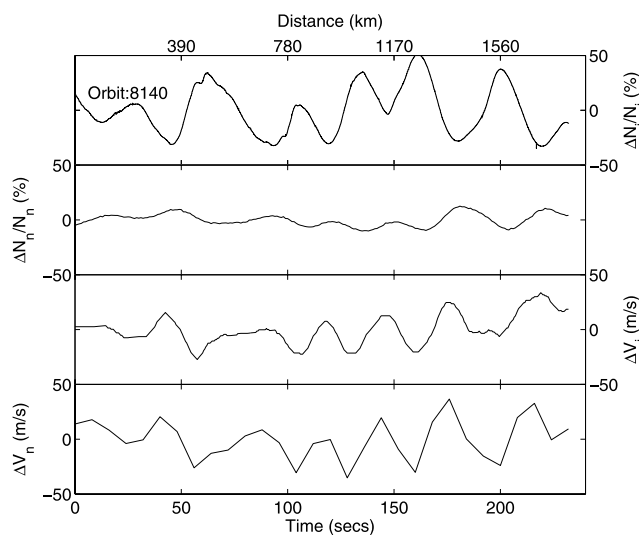


Figure 2. The top two panels show the ion (see Figure 1) and neutral density perturbations for orbit 8140, respectively. The third and fourth panels display the corresponding linearly detrended ion and neutral vertical velocities.

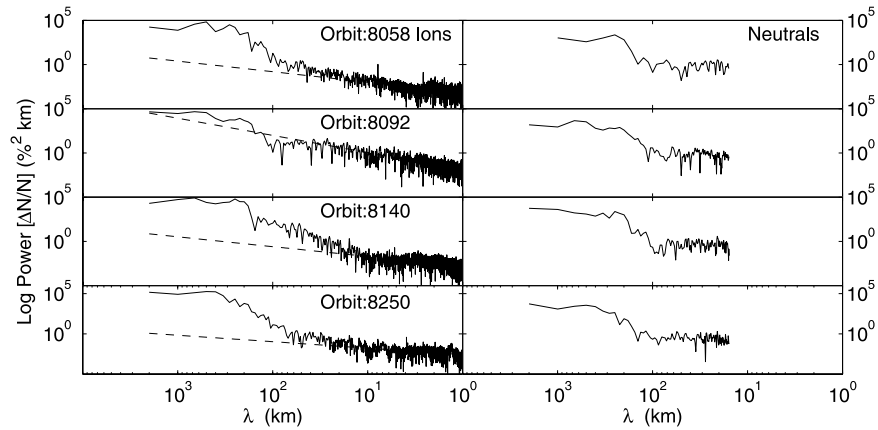


Figure 3. The left panels show the plasma density perturbation spectra for the four orbits shown in Figure 1. The corresponding neutral density spectra are shown in the right panels. The dashed line is a power law fit to the plasma density over the 1–10 km wavelength range.

c in Figure 4 show the dissipation height (z_{diss}), which is defined as the altitude at which the momentum flux profile has its peak value [Vadas and Fritts, 2006]. Panels b and d show the altitude at which the momentum flux is attenuated by a factor of two above z_{diss} . The main effects of the background neutral wind field are to shift the horizontal wavelength of the waves that are most effective at reaching F region altitudes from a range of ~ 100 – 150 km (for no background wind field) to ~ 200 – 250 km (for a typical background wind field of 150 m/s), and to increase the altitude range at which the wave energy is dissipated by about 75 km, from ~ 200 km to ~ 275 km.

4. Discussion

[17] The fact that the neutral density fluctuations shown in Figure 2 lag the neutral vertical velocity by ninety degrees (phase quadrature) implies that these perturbations are gravity waves [Hines, 1960]. Furthermore, the anti-correlation of the neutral and plasma densities shown in the figure is common to all the orbits in which large scale density perturbations are observed, and is consistent with the hypothesis that gravity waves are responsible for the observed plasma perturbations. The relative magnitudes of the physical forcing terms that produce this anti-correlation can be further investigated using the ion continuity equation:

$$\frac{\partial N_i}{\partial t} = -N_i(\nabla \cdot \mathbf{V}_i) - \mathbf{V}_i \cdot \nabla N_i + Q - L \quad (2)$$

where N_i is the ion density, \mathbf{V}_i is the ion velocity, L is the chemical loss rate, t is time, and Q is the production term. Since the observations presented here are all from nighttime midlatitudes, Q may be set to zero for estimation purposes. For an incompressible fluid the first term on the right hand side is also zero, so the time rate of change of the ion density is due to the combination of ion transport and chemical loss. Both of these processes are quantified below using a combination of model values and measurements; through this approach the relative importance of each mechanism can be identified.

[18] In the case of ion transport the upward or downward motion of the neutrals displaces the ions through direct

collisional processes. Since the background neutral density decreases exponentially with altitude, the neutral density gradient points downward on the bottomside of the F region. In contrast, the plasma density gradient at altitudes below the F peak is upward. Consequently a net upward drift of the neutral atmosphere will increase the neutral density at a given altitude, but as the displaced neutrals drag the F region ions to higher altitudes the ion density at the same altitude will decrease. Downward motion of the neutrals will have the opposite effect, so the ion and neutral density fluctuations will be consistently anticorrelated. However, this anticorrelation will also be affected by chemical recombination, which is enhanced at a given altitude when upwelling causes the local neutral concentration to increase. This chemical effect could be somewhat cumulative over time, since there is no offsetting production enhancement during the downgoing wave phases. It is also worth noting that transport cannot be the only active process, because this leads (through equation (2)) to phase quadrature between V_i and N_i , and the observations shown in Figure 2 do not consistently show such a relationship.

[19] Figure 2 does reveal that the relative fluctuations in the plasma density are roughly three times larger ($\sim 30\%$) than the corresponding fluctuations in the neutral density ($\sim 10\%$). This 3-to-1 ratio is in agreement with theoretical expectations for gravity wave-driven perturbations at bottomside F region altitudes [D. Fritts, personal communication]. Note that one might expect to observe offsets in the measured ion and neutral density anticorrelations because the ion motions are constrained by the geomagnetic field lines but the neutrals are not. However, at midlatitude dip angles these offsets are comparable to the calculated vertical displacement of the medium, which is approximately 6 km (see below). Such offsets are much smaller than the horizontal wavelengths observed, and correspond to temporal offsets of less than one second in the data samples.

[20] The International Reference Ionosphere (IRI) model [Bilitza, 2001] for conditions relevant to the time and location (latitude and altitude) of the observations yields an ionospheric density near $1.5 \times 10^5 \text{ cm}^{-3}$ and an upward directed density gradient of about $6.2 \times 10^3 \text{ cm}^{-3} \text{ km}^{-1}$ at 275 km, which is the average altitude of the wave obser-

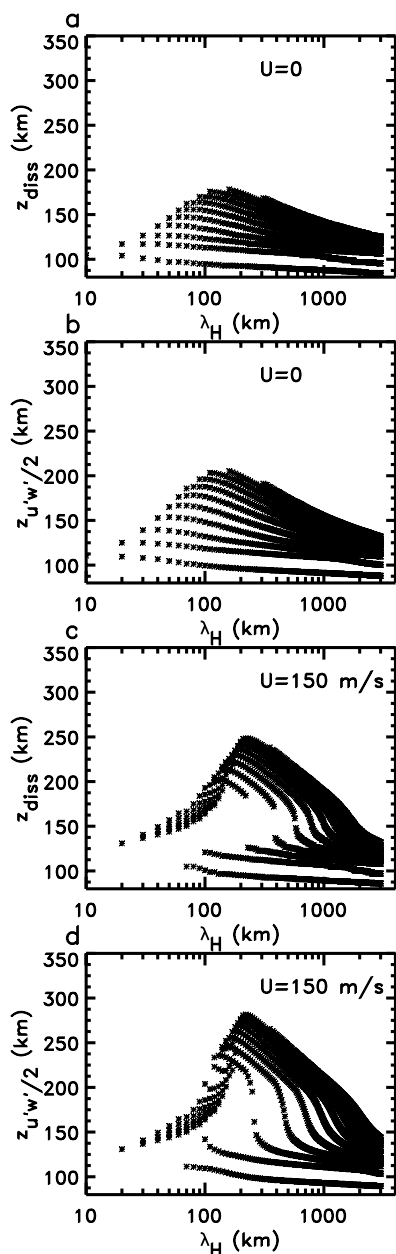


Figure 4. Model data illustrating the penetration altitudes for the energy and momentum of a white noise gravity wave spectrum incident on the thermosphere from below. Panels a and b correspond to a case with no horizontal neutral wind, and panels c and d show the results when a horizontal neutral wind of 150 m/s is imposed.

variations. In order for this gradient to produce a 30% fluctuation in the plasma density it must correspond to a vertical displacement in the *F* region of ~ 6 km. If the vertical velocity is assumed to vary sinusoidally in time, then this vertical displacement for the upwelling quarter wave cycle should equal $AT/2\pi$, where A is the amplitude of the vertical velocity perturbation and T is the wave period. Plugging in 20 m/s for A (see Figure 2) gives a period of 31 min, which is reasonable for a gravity wave at these altitudes. Since the gravity waves propagating to the highest altitudes in the thermosphere propagate against the

winds [Vadas and Fritts, 2006], a 30 minute period corresponds to an intrinsic period of 10–20 minutes for typical thermospheric winds; these intrinsic periods are consistent with the penetration to 275 km altitudes [Vadas, 2007]. The horizontal phase speed for the waves is likely on the order of 100–200 m/s, but unfortunately this cannot be verified using the satellite data. Determination of horizontal phase speeds for gravity waves is more easily done with ground-based optics or radar observations [Oliver *et al.*, 1997; Kelley *et al.*, 2000].

[21] Using the vertical perturbation velocity from Figure 2 allows the rate of change of the ion density due to transport to be estimated. Plugging in 20 m/s for the vertical velocity (V_i) and $6.2 \times 10^3 \text{ cm}^{-3} \text{ km}^{-1}$ for the vertical density gradient in equation (2) yields a loss rate due to transport of $124 \text{ cm}^{-3} \text{ s}^{-1}$. At this rate the observed plasma density perturbations will be produced in about four minutes.

[22] Chemical processes can also produce anti-correlations between the ion and neutral densities. If the neutral atmosphere is locally displaced upwards from its equilibrium altitude by a gravity wave, then the recombination rate of ions in the *F* region will increase due to the larger concentration of neutral particles with which to react. The pacing reactions in the loss of O^+ in the bottomside *F* region are the charge exchange processes with N_2 and O_2 , which have reaction rates of about 1.1×10^{-12} and $2.0 \times 10^{-11} \text{ cm}^3 \text{ s}^{-1}$, respectively. Figure 2 shows that the average change in the neutral density due to the wave is about 10%. From the combined charge exchange reactions, the net loss rate of O^+ due to a 10% increase in the neutral densities of N_2 and O_2 at the altitude of the satellite is about $35 \text{ cm}^{-3} \text{ s}^{-1}$. This is slightly more than one-fourth as large as the rate derived above for the transport process.

[23] The change in the chemical reaction rates due to temperature variations induced by gravity waves at these altitudes can also affect the loss rate, but this change is much smaller than that calculated above. A similar loss rate calculation reveals that temperature induced changes in the recombination rates for the reactions that remove O^+ from the *F* region would require 35–40 min to produce the observed variations in the ion density.

[24] The above estimates show that the observed changes in the ion density are primarily due to collision-induced transport of ionization by a gravity wave. For reasonable gravity wave parameters the transport effect is almost four times faster than chemical recombination. However, since the two effects are the same order of magnitude, and since both lead to anticorrelation of the density perturbations on the bottomside *F* region, both terms should be considered in any numerical simulation of the effects of gravity waves on the nighttime ion density distribution.

[25] Another interesting feature of the data is the cut-off near horizontal wavelengths of 100–200 km in the power spectra shown in Figure 3. Because of the high inclination of the DE-2 orbit, the horizontal wavelengths of the observed density perturbations are only indicative of actual wave scale lengths if the waves that create the perturbations are propagating in the meridional direction. For any other propagation direction the apparent wavelength will be longer. Oliver *et al.* [1997] show that the majority of gravity waves observed by the MU radar in Japan propagate from north to south, but they also show a significant number of

wave observations with northward and east-west propagation directions. Assuming that the observed midlatitude perturbations in the densities measured by DE-2 are due to gravity waves, then the random orientation of these waves relative to the orbit plane will produce density irregularity spectra with wavelengths greater than or equal to the fundamental scale length at which the energy is incident.

[26] The gravity wave dissipation model described by *Vadas and Fritts* [2005] agrees well with the DE-2 measurements in two important ways. First, for a white noise gravity wave input the model results in Figure 4 show a strongly peaked spectral response at the altitudes of interest, with wavelengths of the largest waves centered at 100–250 km. The cut-offs in the DE-2 plasma and neutral density spectra near wavelengths of 100–200 km are therefore consistent with the model prediction, since the observed wavelengths are greater than or equal to the cut-off given by the model.

[27] The second significant source of agreement between the data and the model is the altitude to which the waves from the lower atmosphere penetrate before dissipation. Since the specific thermospheric wind profiles during the events observed by DE-2 are unknown, MSISE-90 and TIME-GCM model temperature and wind profiles corresponding to the average latitudes and local times of the observations are used to provide the background characteristics for the gravity wave propagation model. It is worth noting that the background wind and the presence of shears in the wind profile are strong factors in the upward propagation and filtering of gravity waves, and these are important factors in the model. For average conditions the model results shown in Figure 4 predict that there will be essentially no signature of incident gravity waves at altitudes greater than a few scale heights above the dissipation altitude [*Vadas*, 2007]. This result suggests that such gravity waves may usually be undetectable at altitudes much greater than 300 km, which explains why such observations from satellites are relatively rare.

[28] It is unlikely to be coincidental that in the entire 18 month DE-2 data set there are no wave signatures similar to those shown in Figure 1 until the very last month of the satellite's life, at which point the orbit had decayed so that perigee was below 300 km. There are no major geophysical differences between the final month of the satellite's life and the preceding months, therefore the observed effect is likely indicative of an altitude cut-off in the gravity wave propagation characteristics, as the model predicts.

5. Summary and Conclusions

[29] Midlatitude measurements from late in the life of the polar orbiting DE-2 satellite are consistent with the idea of gravity waves incident on the ionosphere causing large perturbations in the local plasma density at altitudes below the *F* region peak. The horizontal scale sizes of the plasma and neutral density structures are observed to be longer than 100–200 km, with fluctuation amplitudes ($\Delta N/N$) for the plasma that average about 30% of the background density. The neutral fluctuation amplitudes are about a third as large, which is consistent with expectations based on the scale heights of the plasma and neutral gases. The physical picture confirms the idea that gravity waves incident on

the ionosphere from below produce net upward and downward displacement of the quiescent neutral and plasma background density profiles, resulting in local enhancements and depletions of the densities at the satellite location. Enhancements in the neutral density correlate with depletions in the plasma density (and vice versa) due to the oppositely directed background density gradients at the altitudes of the observations. Chemical recombination reactions resulting from the gravity wave-induced displacement of the neutral atmosphere are also important, but require about four times as long as transport effects to produce the same level of ion density fluctuations.

[30] The wavelike features are never observed at altitudes above ~ 300 km at midlatitudes, but are frequently observed below this height. A wave period of ~ 30 min is consistent with the observed density fluctuations for vertical perturbation velocities near 20 m/s. Both the horizontal wavelength and the dissipation altitude predicted by the gravity wave dissipation model of *Vadas and Fritts* [2005] and *Vadas* [2007] agree well with the observations, assuming propagation through a model atmosphere consistent with average conditions for the same altitude, latitude, and geophysical conditions. Thus the DE-2 observations provide strong empirical validation of the model predictions, and indicate that the presence of such waves at midlatitudes may be quite common, but only below altitudes of about 300 km.

[31] **Acknowledgments.** This work was supported by NSF grants ATM-0535358 and ATM-0537311, and by NASA under contract NNH07CC81C. The authors thank Arthur Richmond and David Fritts for helpful discussions.

[32] Zuyin Pu thanks Timothy Kane and another reviewer for their assistance in evaluating this paper.

References

- Bilitza, D. (2001), International reference ionosphere 2000, *Radio Sci.*, *36*, 2, 261.
- Bishop, R. L., N. Aponte, G. D. Earle, M. Sulzer, M. F. Larsen, and G. S. Peng (2006), Arecibo observations of ionospheric perturbations associated with the passage of tropical storm Odette, *J. Geophys. Res.*, *111*, A11320, doi:10.1029/2006JA011668.
- Dubey, S., R. Wahi, and A. K. Gwal (2006), Ionospheric effects on GPS positioning, *Adv. Space Res.*, *38*, 2478, doi:10.1016/j.asr.200507.030.
- Earle, G. D., A. M. Musumba, and J. P. McClure (2006), A global study of nighttime midlatitude topside spread echoes, *J. Geophys. Res.*, *111*, A11306, doi:10.1029/2006JA011614.
- Fukao, S., M. C. Kelley, T. Shirakawa, T. Takami, M. Yamamoto, T. Tsuda, and S. Kato (1991), Turbulent upwelling of the mid-latitude ionosphere 1. Observational results by the MU radar, *J. Geophys. Res.*, *96*, 3725.
- Gross, S. H., C. A. Reber, and F. T. Huang (1984), Large-scale waves in the thermosphere observed by the AE-C satellite, *IEEE Trans. Geosci. Remote Sens.*, *GE-22*, 340.
- Hanson, W. B., R. A. Heelis, R. A. Power, C. R. Lippincott, D. R. Zuccaro, B. J. Holt, L. H. Harmon, and S. Santini (1981), *Space Sci. Inst.*, *5*, 503–510.
- Hedin, A. E. (1991), Extension of the MSIS thermosphere model into the middle and lower atmosphere, *J. Geophys. Res.*, *96*, 1159.
- Hedin, A. E., and H. G. Mayr (1987), Characteristics of wavelike fluctuations in dynamics explorer neutral composition data, *J. Geophys. Res.*, *92*, 11,159.
- Heelis, R. A., W. B. Hanson, C. R. Lippincott, D. R. Zuccaro, L. H. Harmon, B. J. Holt, J. E. Doherty, and R. A. Power (1981), The ion drift meter for dynamics explorer-B, *Space Sci. Instrum.*, *5*, 511.
- Hines, C. O. (1960), Internal atmospheric gravity waves at ionospheric heights, *Can. J. Phys.*, *38*, 1441.
- Hysell, D. L. (2000), An overview and synthesis of plasma irregularities in equatorial spread F, *J. Atmos. Sol. Terr. Phys.*, *62*, 1037.
- Johnson, F. S., W. B. Hanson, R. R. Hodges, W. R. Coley, G. R. Carignan, and N. W. Spencer (1995), Gravity waves near 300 km over the Polar caps, *J. Geophys. Res.*, *100*, 23,993.
- Kelley, M. C., J. J. Makela, W. E. Swartz, S. C. Collins, S. Thonnard, N. Aponte, and C. A. Tepley (2000), Caribbean ionosphere campaign,

- year one: Airglow and plasma observations during two intense mid-latitude spread-F events, *Geophys. Res. Lett.*, *27*, 2825.
- Oliver, W. L., Y. Otsuka, M. Sato, T. Takami, and S. Fukao (1997), A climatology of F region gravity wave propagation over the middle and upper atmosphere radar, *J. Geophys. Res.*, *102*, 14,499.
- Spencer, N. W., L. E. Wharton, H. B. Niemann, A. E. Hedin, G. R. Carignan, and J. C. Maurier (1981), The dynamics explorer wind and temperature spectrometer, *Space Sci. Instrum.*, *5*, 417.
- Vadas, S. L. (2007), Horizontal and vertical propagation and dissipation of gravity waves in the thermosphere from lower atmospheric and thermospheric sources, *J. Geophys. Res.*, *112*, A06305, doi:10.1029/2006JA011845.
- Vadas, S. L., and D. C. Fritts (2005), Thermospheric responses to gravity waves: Influences of increasing velocity and thermal diffusivity, *J. Geophys. Res.*, *110*, D15103, doi:10.1029/2004JD005574.
- Vadas, S. L., and D. C. Fritts (2006), Influence of solar variability on gravity wave structure and dissipation in the thermosphere from tropospheric convection, *J. Geophys. Res.*, *111*, A10S12, doi:10.1029/2005JA011510.
- Yunck, T. P. (1993), Coping with the Atmosphere and Ionosphere in Precise Satellite and Ground Positioning, in *Environmental Effects on Spacecraft Positioning and Trajectories*, edited by A. Valence Jones, *Geophys. Monograph*, *73*, AGU, Washington, D. C.

G. D. Earle and A. M. Musumba, William B. Hanson Center for Space Sciences, University of Texas at Dallas, WT-15, Richardson, TX 75083, USA. (earle@utdallas.edu)

S. L. Vadas, NorthWest Research Associates, CoRA Division, Boulder, CO, USA.